Pierre Magnier

Vincent Boucinha

Laboratoire de Mécanique et d'Énergétique,
8 Rue Léonard de Vinci,
45072 Orléans, Cedex 02, France

BinJie Dong
GREMI, UMR 6606,
CNRS/Université d'Orléans,
14 Rue d'Issoudun BP 6744,
45072 Orléans, Cedex 02, France

Régine Weber

Annie Leroy-Chesneau

Laboratoire de Mécanique et d'Énergétique,
8 Rue Léonard de Vinci,
45072 Orléans, Cedex 02, France

Dunpin Hong
GREMI, UMR 6606,
CNRS/Université d'Orléans,
14 Rue d'Issoudun BP 6744,
45072 Orléans, Cedex 02, France

Experimental Study of the Flow Induced by a Sinusoidal Dielectric Barrier Discharge Actuator and Its Effects on a Flat Plate Natural Boundary Layer

Since the mid-1990s, electrohydrodynamic actuators have been developed for modifying on subsonic airflows. The principle of plasma action is the use of the direct conversion of electrical energy into kinetic energy in order to act on the flow boundary layer. This paper presents our contribution to such an investigation concerning an electrohydrodynamic actuator consisting of several sinusoidal dielectric barrier discharges. First, the ionic wind induced by this actuator was measured with a pressure sensing probe. The induced flow velocity increased with the applied voltage and frequency. The particle image velocimetry system without external airflow showed the presence of induced swirls, generated by the ion movement in plasma. Then the action of this actuator on a flat plate boundary layer in parallel flow at zero incidence was studied in a subsonic wind tunnel. Experiments were performed for 15 m/s and 22 m/s. They showed that electric discharges (±8 kV, 1 kHz) acting on a laminar flow tripped the laminar-to-turbulent transition. Moreover, higher applied voltages (up to ±12 kV, 1 kHz) were necessary for modifying turbulent boundary layers. [DOI: 10.1115/1.3026722]

Keywords: boundary layer, dielectric barrier discharge, electrohydrodynamics, plasma actuator

1 Introduction

The subsonic flow control can have an important impact on industry. Main objectives are to remove the negative effects of a flow as the reduction of noise or drag decreases, and to improve the positive effects as the lift or fluid mixture increases. It could improve aerodynamic performances of transport vehicles to have higher velocities for lower energy consumption. For example, in the case of military aircrafts, stall angle delay may improve maneuver possibilities. Turbulent boundary layer presents a high velocity gradient on the wall. Then it allows the flow to better resist unfavorable pressure gradients, and thus to not separate from the wall. Thus classical methods of flow control are based on actions on the boundary layer laminar-to-turbulent transition and modifications of the wall friction. Two kinds of action are investigated. Passive methods consist of modifying the wall conditions for promoting transition, such as riblets [1] and vortex generators [2]. Active methods of flow control consist of inducing flow perturbations in the vicinity of the wall, such as moving surface [3], blowing, and suction with periodic excitation [4] among others.

For this purpose, nonthermal plasmas have been studied since the mid-1990s for their use in aerodynamics [5]. Several experimental and numerical investigations have shown the ability of plasma actuators for modifying subsonic airflows. The principle is to use the ionic wind induced by electric discharges [6], with a direct conversion of electrical energy into mechanical energy. The advantages of plasma actuators are no mechanical parts and a short response time. dc corona discharges in steady mode were developed by several authors [7–14] for airflow control. It enabled reductions of flow separation on a NACA 0015 airfoil up to Re =267 K and angles of attack up to 17.5 deg [15]. More efficient actuations were obtained by using different working modes, other electric sources, and/or other geometrical configurations. Indeed, plasma actuators based on dielectric barrier discharge (DBD), supplied by an ac electric source, were developed in Refs. [16–22]. These references used a steady actuation on the flow and significantly acted on airflows, but better effects were achieved with unsteady actuation. Sosa et al. [23] employed a dc corona discharge working in an unsteady mode for delaying the flow separation. By adjusting the applied signal frequency, they acted for Reynolds numbers of up to 333 K. Corke and co-workers [24,25] and Post et al. [26] used ac unsteady DBDs to delay the airfoil stall for Reynolds numbers of up to 584 K. Opaits et al. [27] acted up to 75 m/s on an 8-cm wide airfoil. Plasma actuator placed at the airfoil leading edge has similar effects to leading edge slats, and similar to flaps when it is placed at the trailing edge [25]. A review of the main reported works was done by Moreau [28]. Most authors estimate that the effect of plasma actuators on an airflow is mainly due to the ionic wind, but thermal effects (gas heated by discharges) may also affect the physical properties of the air [29].

However, the plasma-airflow interaction and the effects on boundary layers are not clearly fixed. Therefore, in order to have a better understanding of how to act with plasma on wall-bounded flows, we present in this paper the investigation of a typical natural evolving boundary layer on flat plate and its modifications by an actuator based on multi-DBDs working in steady mode. For this purpose, Velkoff and Ketcham [30] used four successive wires generating corona discharges and shifted the laminar-to-turbulent transition at about 50 m/s. Grundmann and Tropea [31] also delayed transition on a 1.6-m long flat plate at 6 m/s, with two successive DBD actuators. Moreau et al. [32] modified veloc-

Contributed by the Fluids Engineering Division of ASME for publication in the JOURNAL OF FLUIDS ENGINEERING. Manuscript received July 16, 2007; final manuscript received October 9, 2008; published online December 2, 2008. Assoc. Editor: James A. Liburdy.

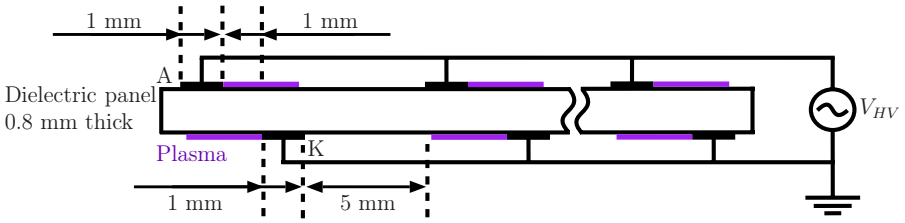

Fig. 1 Actuator with several dielectric barrier discharges

ity profiles and induced a drag reduction on a 30-cm long flat plate with a dc surface corona discharge of up to 25 m/s. Porter et al. [33] used a single DBD for tripping the laminar-to-turbulent transition of a flat plate boundary layer at 4 m/s and 6.5 m/s. Numerical investigations of boundary layer control by electric discharges have shown the ability to strongly modify velocity profiles [34,35]. The investigated plasma actuator in the present study consisted of successive DBDs. The plasma process of this kind of electric discharge was developed by Enloe et al. [19], Van Dyken et al. [36], and Likhanskii et al. [37]. First, the flow induced by this actuator was studied without external flow with the particle image velocimetry (PIV) system for various applied voltages and frequencies. In order to act on laminar then turbulent natural evolving boundary layers, this actuator was then mounted on a 1-m long flat plate and acted at ±8 kV and 1 kHz in various positions. Inlet airflow velocities were 15 m/s and 22 m/s. Velocity profile measurements were performed in numerous positions along the flat plate at zero incidence and evolution of characteristic boundary layer parameters were deduced.

2 Experimental Setup

2.1 Plasma Actuators and Power Supply. The plasma actuator consisted of several dielectric barrier discharges established on a dielectric material ($160\times115\times0.8$ mm^3). The actuator was realized with a printed circuit board (PCB). Each DBD was created between two thin copper electrodes (width of 1 mm, thickness of 35 μm) separated by a dielectric panel in epoxy, see Fig. 1. These electrodes had an asymmetric design with a 1 mm gap between the upper and lower electrodes. The gap between two pairs of electrodes was 5 mm. Measurements with the particle image velocimetry system, shown in Sec. 3.2, were performed with an actuator consisting of 12 successive single DBDs. Induced velocity profiles and action on a flat plate boundary layer were studied with 15 single DBDs. The plasma power consumption was between 7 W and 60 W for the entire actuator (see Table 1). Parametric studies of this kind of actuator geometry were done by Borghi et al. [38], Forte et al. [39] and Magnier et al. [40].

The upper electrodes were connected to an ac power supply, described in Fig. 2. A sound amplifier (Crown®, Xs1200, 0.022–22 kHz, 2.3 kW) magnified the sine waveform delivered by a function generator. Voltage of amplitudes of up to ±20 kV (i.e., 40 kV peak to peak) was obtained with a high voltage transformer (90 V/20 kV, up to 20 kHz). The power supply output voltage was measured with a high voltage probe Tektronix P60115A. Outputs were visualized with a fast digital oscilloscope LeCroy WaveSurfer 454. The lower actuator surface, with electrodes connected to the ground, was covered with a thin layer of Kapton®, in order to inhibit discharges on the grounded side. Plasma actuators worked in steady mode. The typical behavior of the discharge current versus time for a sine high voltage is shown in Fig. 3 (±5 kV, 1 kHz). It shows that the positive discharge consists of successive streamers whereas the negative discharge is more homogeneous.

Table 1 Maximum induced flow velocity for various active powers, 1 mm behind the last electrode

±8 kV	P (W)	U_p (m/s)
0.5 kHz	10.56	1.48
1 kHz	22.99	2.38
2 kHz	42.53	3.06
1 kHz	**P (W)**	**U_p (m/s)**
±6 kV	7.40	1.53
±8 kV	22.99	2.38
±10 kV	38.80	2.95
±12 kV	61.48	3.25

2.2 Flat Plate. In order to investigate modifications of the boundary layer due to the plasma actuator, we used a 1-m long, 300-mm broad, and 30-mm thick flat plate made entirely of polyvinyl chloride (PVC) (Fig. 4). It was divided into three parts, fixed with electrically insulating screws (Nylon®). The flat plate leading edge was a NACA 0015 leading edge (0–30% chord, 60 mm long) since it presents no bubbles at 0 deg for the investigated velocities. The flat plate trailing edge was a NACA 0015 trailing edge (30–100% chord, 140 mm long). Four plasma actuators, each one constituted of 15 single DBDs, were placed in slots separated 13 mm away from the medium part, as described in Fig. 4. The flat plate surface was then quasismooth (the electrode thickness of

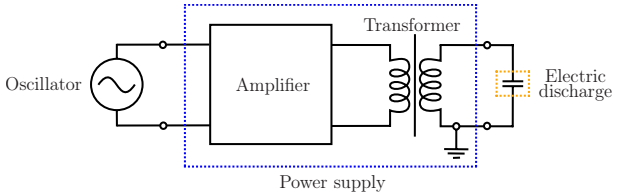

Fig. 2 Power supply for the DBD actuator

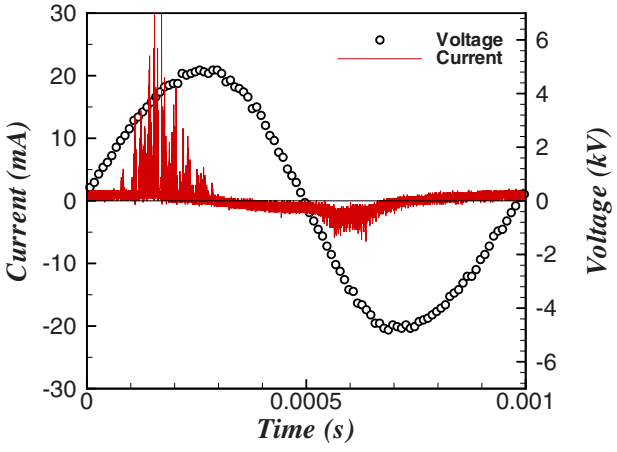

Fig. 3 Voltage and current versus time (±5 kV, 1 kHz)

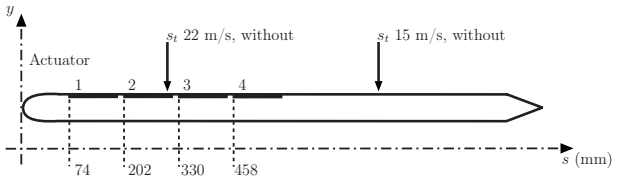

Fig. 4 Schematic of the flat plate with positions of four DBD actuators

35 μm was negligible [41]). All plasma actuators were oriented in order to generate an ionic wind in the same direction as the main flow.

The curvilinear abscissa s is used for determining positions on the flat plate, in order to take into account of the leading edge curvature. The y-axis origin is the flat plate surface, and the s-axis origin is the flat plate leading edge.

2.3 Subsonic Wind Tunnel. Experiments with the flat plate were performed in a subsonic open-circuit wind tunnel with a 2-m long square test section (50×50 cm^2), described in Fig. 5. The nozzle has a section contraction ratio of 1:16. The maximum velocity is about 50 m/s, generated by a 30 kW electric fan. Flow characterization with a hot wire probe indicated that the mean turbulence ratio was 0.4% in the beginning of the test section, without an obstacle, and the flow was bidimensional over 85% of the wind tunnel test section height and width. The 1-m long plate with actuators was placed between two vertical plates (1.5 m $\times$50 cm$\times$15 mm) in order to limit tridimensional effects.

2.4 Flow Measurements

2.4.1 Particle Image Velocimetry System. Flow velocity fields were determined using the PIV system. A laser sheet was generated from a laser beam (wavelength of 532 nm, Nd:Yag laser, Big Sky Laser) using mirrors and lenses, and illuminated smoke particles, which seeded the airflow. A charge coupled device camera PowerView Plus TSI (model 630159) captured images of illuminating particles (2048×2048 pixels^2). Displacement vectors of each particle were then calculated by InSight™ using two successive images recorded for two successive laser pulses (200 mJ each, time delay of 10 μs). The velocity fields presented in this paper are the mean vector fields of 500 pairs of such recorded images.

2.4.2 Pressure Sensing Probe. In order to avoid unwanted electrical arcs, a total pressure probe made of glass was used (external diameter of 0.6 mm, internal diameter of 0.4 mm). The lower vertical measurement position was thus 0.3 mm on the y-axis. In order to have velocity measurements, a static pressure probe was fixed to the glass probe. This pressure measurement system was calibrated with a classical Pitot tube in a subsonic wind tunnel. The error made in pressure measurements is under 0.5% for a probe rotation of ±7.5 deg.

For the induced flow velocity measurements in Sec. 3, the pressure measurement system was connected to a differential low-

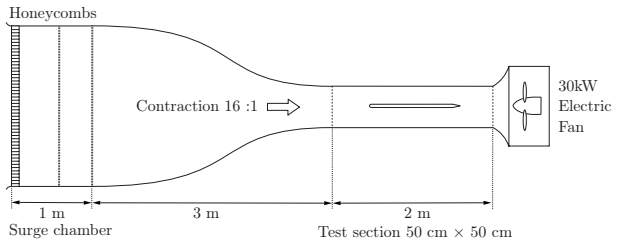

Fig. 5 Subsonic wind tunnel with a square test section of 50 cm$\times$50 cm$\times$2 m

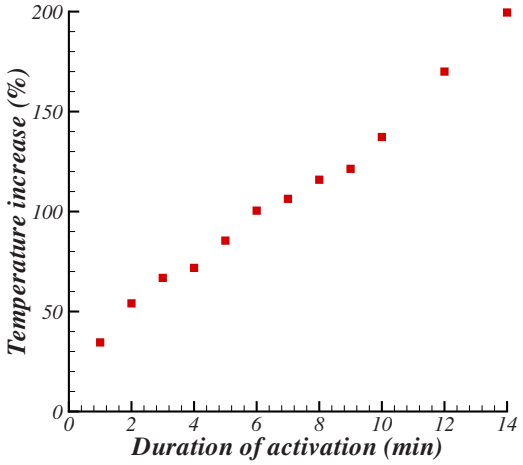

Fig. 6 Actuator temperature increase during its activation duration (initial actuator temperature of 22°C)

pressure transducer Druck™ LPM 9481 with a short pressure brand of 0–20 Pa (output voltage 0–5 V) in order to precisely measure low velocities. For flat plate boundary layer investigations in Sec. 4, the pressure measurement system was connected to a differential pressure transducer Druck™ LPM 9381 with a wider pressure brand of 0–500 Pa (output voltage of 0–5 V). The measurement accuracy of these transducers was 0.1% of the full range. Measurements were acquired on a PC using a 16-bit acquisition card (resolution of the output voltage measured at 8×10^{-5} V, i.e., ±0.008 Pa), over a 1 s interval at a 3 kHz sampling rate. Velocity profiles were obtained from time-averaged pressure measurements.

This velocity measurement system was fixed to a computer controlled two-dimensional traversing system Isel® Automation LF 5 (displacement precision of ±0.02 mm).

2.4.3 Test Procedure. Without external airflow, because of plasma inhibition on the grounded side, an important part of the applied power was dissipated into the dielectric material. The temperature on the actuator surface increased from 22°C to 66°C after an activation duration of 14 min (+200%), as shown in Fig. 6 (measured with a surface thermometer TESTO, from −50°C to 250°C). A test procedure was chosen in order to verify that dielectric surface heating did not produce a notable effect on the flow. It consisted of measuring a velocity profile without activated plasma in a position s, and then velocity profile measurement was performed in the same position with the working actuator. Since the duration of each velocity profile measurement was about 8 min, a velocity profile without discharge was measured and compared with the natural boundary layer after each measurement with plasma. There was no difference between these two profiles without plasma. Therefore dielectric surface heating does not produce a notable effect on the flow.

During these experiments, velocity profiles were measured every 16 mm along the s-axis until the fourth actuator, and every 50 mm downstream. Their heights were measured up to 20 mm in the y-axis.

Temperature in the test section, atmospheric pressure, and relative humidity were recorded for each velocity profile (thermohygrometer Kimo®, HD 100), for determining air density ρ and dynamic viscosity μ.

3 Flow Induced by the Plasma Actuator

First, this actuator was studied without external airflow in order to characterize the flow induced by the successive DBDs.

3.1 Induced Flow Velocity Profiles. The velocity of the induced ionic wind was measured for various voltages (from

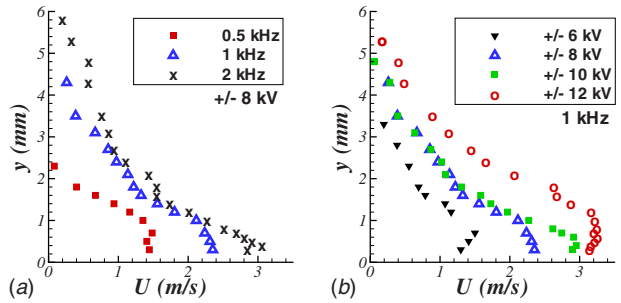

Fig. 7 Induced flow velocity, 1 mm after the last electrode (*a*) for various frequencies (0.5 kHz, 1 kHz, and 2 kHz) and a given applied voltage of ±8 kV, and (*b*) for various high voltages (from ±6 kV to 12 kV) and a given frequency of 1 kHz

±6 kV to ±12 kV) and frequencies (0.5 kHz, 1 kHz, and 2 kHz) of the applied signal. Induced flow velocity profiles, without external airflow, were performed 1 mm behind the last 15th single DBD. Figure 7 shows the measured curves and maximum velocities U_p of induced flow are reported for each case in Table 1.

For a given frequency, the maximum velocity of the plasma-induced flow increased with the voltage amplitude. Indeed, the phenomenon of ionization was more important, therefore more ions moved in the interelectrode space. The momentum transfer with the neutral molecules was more important, and the flow resulting from it was thus faster. Moreover for a given voltage, the velocity was more important when the frequency of the signal increased. Thus to obtain the maximum velocity for this actuator, the frequency and the voltage must be the highest possible voltage according to the power supply limitations.

3.2 Induced Flow Topology. In order to study the induced flow topology on the actuator, measurements with the PIV system were performed without external airflow. The measurement window in Fig. 8 shows the flow streamlines above the last six single DBD (12 couples, gap of 8 mm between two DBD), for 1 kHz and two voltage amplitudes, ±5 and ±12 kV.

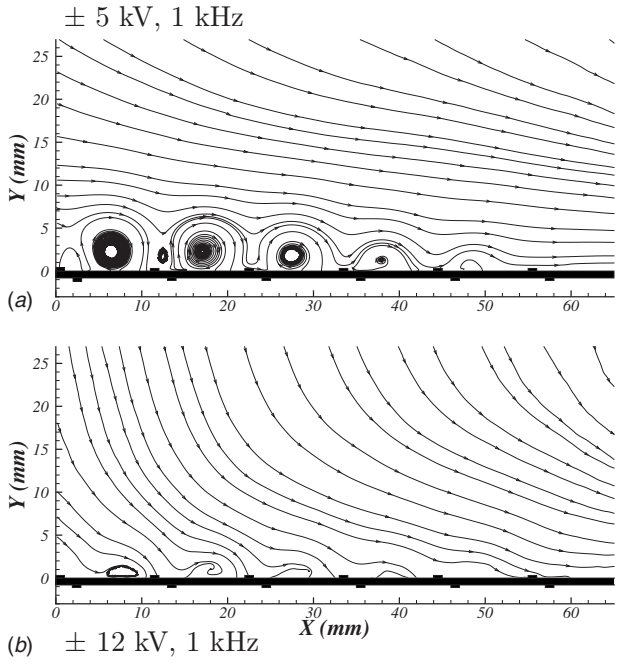

Fig. 8 Flow streamlines induced by the DBD actuator with a frequency of 1 kHz and a voltage of (*a*) ±5 kV and (*b*) ±12 kV

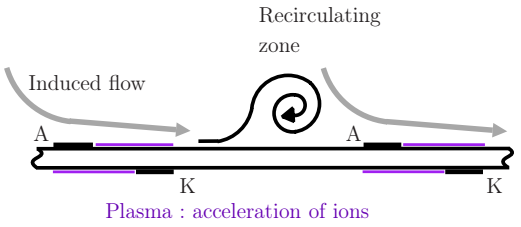

Fig. 9 Schematic of the flow induced by a DBD actuator

This figure shows swirls in space between two pairs of electrodes. The position and the rotation direction of these swirls indicate the way in which the neutral molecules of gas are involved. For each DBD, ions generated by the high voltage move in the interelectrode gap. This movement is very close to the actuator surface (the ion sheath size is up to 50 μm [42]). Some neutral molecules of gas in the direct vicinity of the plasma are thus involved by momentum transfer with ions in the interelectrode space (model of "porous piston" by Likhanskii et al. [37]). These molecules are strongly accelerated near the plasma and induce a flow. It pulls down above the plasma and goes down toward the anode. The global flow movement, resulting from positive and negative half-cycles, is directed from the exposed anode toward the "virtual" cathode (placed on the other side of the dielectric panel). Downstream of the cathode, there is neither more plasma nor ions to keep on involving the flow. Thus its velocity close to the wall decreases due to the wall friction (null velocity). This induced flow downstream of the first DBD is involved toward the wall by the flow induced by the next DBD since the same flow topology is generated by the next plasma, in particular the flow going down toward the anode. Then this could explain the swirl generation between two DBD (Fig. 9).

A part of the flow induced by the first DBD is accelerated by the second one. The flow is then faster downstream this second DBD and is less affected by the flow induced by the next plasma. The size of the swirls is then increasingly reduced along the longitudinal axis. The flow is accelerated after each couple of electrodes, which confirms the observations made by Forte et al. [39].

Moreover, more ionized plasma (generated by the higher applied voltage) induces a faster flow compared with lower applied voltages. The size of swirls for ±12 kV is thus reduced in comparison with ±5 kV.

4 Action of the Plasma Actuator on a Boundary Layer

4.1 Curves and Results. Experiments with external airflow, in the subsonic wind tunnel described in Sec. 2.3, were performed on a 1 m flat plate at zero incidence with four plasma actuators (Fig. 4). Natural boundary layers developed along the plate were modified by one of these actuators working at ±8 kV (i.e., 16 kV peak to peak) and 1 kHz. Time-averaged velocity profiles were measured with the pressure sensing probe without and with the actuator working. Each result presented in this paper was validated by comparison with theoretical curves. The action of the third actuator is not shown here because the results are comprised between the results shown for the second and the fourth ones.

Velocity profiles in three positions (s=155 mm, 187 mm, and 427 mm, which showed different kinds of velocity profiles) for two airflow velocities (15 m/s and 22 m/s), without and with activated actuator 1, are shown in Fig. 10. These curves are compared with the Falkner–Skan solutions (laminar boundary layers) and Prandtl's turbulent solution (law in 1/7). Mean airflow velocity, noted U_∞, was determined from the velocity profile in each position.

We consider the nondimensionalized variables u^+ and y^+ defined by the relations $u^+=u/u_\tau$ and $y^+=yu_\tau/\nu$ with u as the

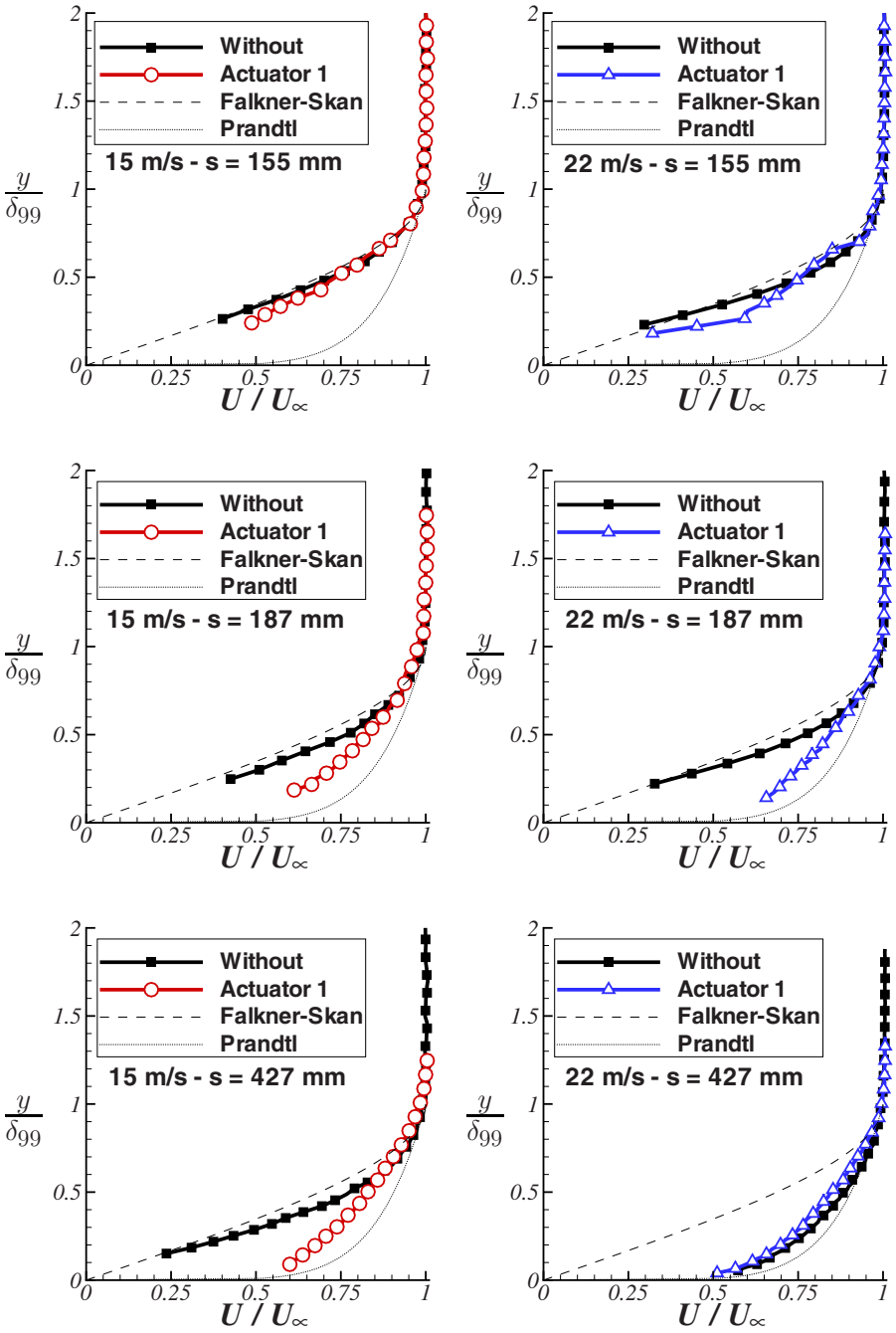

Fig. 10 Nondimensional mean velocity profiles for 15 m/s and 22 m/s, without and with actuator 1 activated (±8 kV, 1 kHz), in *s*=155 mm, 187 mm, and 427 mm

measured velocity at height y. The friction velocity is therefore $u_\tau = \sqrt{(\tau_w/\rho)}$, and the wall shearing-stress is $\tau_w = \mu(\partial u/\partial y)_{y=0}$. The nondimensional mean velocity profiles are plotted on a semilogarithmic scale in Fig. 11, for both velocities and for the three previous positions. These curves are compared with the logarithmic law for turbulent flow [41]: $u^+ = 5.75 \log(y^+) + 5.5$.

From each measured velocity profiles, some characteristic properties were determined as follows:

- the boundary layer thickness δ_{99},
- the displacement thickness $\delta_1 = \int_{y=0}^{\infty}(1 - u/U_\infty)dy$,
- the momentum thickness $\delta_2 = \int_{y=0}^{\infty} u/U_\infty(1 - u/U_\infty)dy$,
- the shape factor $H = \delta_1(s)/\delta_2(s)$,
- and the drag per unit width $D = \rho\int_{y=0}^{\infty} u(U_\infty - u)dy$.

These parameters are plotted along the flat plate in Figs. 12–16, respectively, for each case of actuation. The natural evolving boundary layer parameters are compared with the theoretical laminar evolution (Blasius), and the boundary layer parameters under the action of actuator 1 are compared with the theoretical turbulent evolution (Prandtl). As shown in these figures, the theoretical and experimental curves are similar. But for clearer figures, the theoretical curves are not all plotted. The beginning of the boundary layer turbulent zone s_t is determined for all studied cases by the intersection of the Prandtl turbulent curve with the s-axis on the δ_{99}-graph.

4.2 Effects on a Laminar Boundary Layer. Considering the beginning of the turbulent zone for 15 m/s (s_{t15}=580 mm) in Fig.

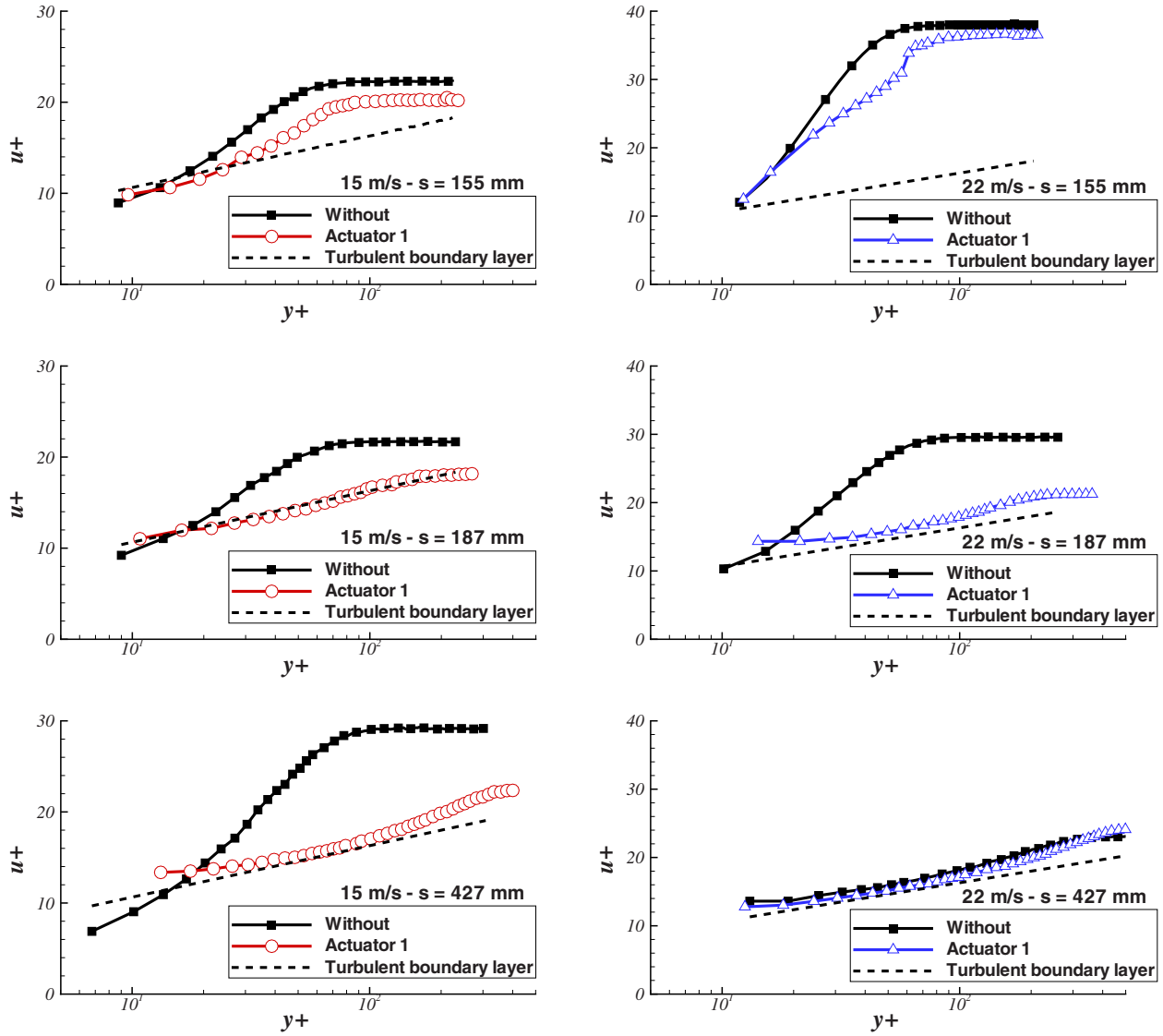

Fig. 11 u^+ **velocity profiles for 15 m/s and 22 m/s, without and with actuator 1 activated (±8 kV, 1 kHz), in** s**=155 mm, 187 mm, and 427 mm**

4, plasma actuators acted on a natural laminar boundary layer. For 22 m/s (s_{t22}=255 mm), the first actuator acted on a laminar boundary layer and the other ones on a turbulent boundary layer.

From Fig. 10, we notice that the boundary layer profiles are modified near to the wall by action of the first actuator in s =155 mm, for both velocities. Then downstream of this position, the velocity gradient on the wall continues to increase along the flat plate, and the forced velocity profiles tend toward the theoretical turbulent solution. We did not notice a clear momentum added by the induced ionic wind on the velocity profiles, as observed for the lower airflow velocity and more powerful discharges by Moreau et al. [32] or Porter et al. [33]. The only visible effect of the plasma actuator on the laminar boundary layer was to make the profiles more turbulent, as shown in Fig. 11. These graphs show that velocity profiles became more turbulent along the plate whereas the natural boundary layer was laminar. Although there was no plasma at position s=427 mm (when actuator 1 was considered), the boundary layer was still turbulent at this position showing that the flow modification was not limited to the place where the actuator was located. Therefore the boundary layer transition was prematurely tripped by the action of the plasma.

The observation of the boundary layer parameters along the flat plate confirms this result. Figures 12–14 show a strong early increase in δ_{99}, δ_1, and δ_2 when actuators are activated. The action of the first actuator on laminar boundary layers for 15 m/s and 22 m/s promoted the transition above this actuator, as shown in Table 2. Moreover the transition was advanced for 15 m/s when the second and fourth actuators were activated. The shape factor H in Fig. 15 strongly decreased above the actuator from the laminar theoretical value (2.59) until the turbulent theoretical value (about 1.4 [41]). This figure clearly shows the beginning of the transition area and the beginning of the boundary layer turbulent zone for each studied case.

Finally, each single DBD of an activated actuator induced an ionic wind, and the effect on a laminar boundary layer was to trip the transition. Each DBD acted as a small turbulator (such as grit paper), which amplified boundary layer instabilities. This succession of disturbances promoted early transition. This remark confirms the experimental results of Porter et al. [33] and the numerical results of Visbal et al. [35]. The main consequence of an earlier turbulent flow on a flat plate was the drag increase, as shown in Fig. 16. Indeed drag was more than tripled (+213%) in s=682 mm for 15 m/s, by action of the first actuator.

4.3 Effects on a Turbulent Boundary Layer. When a plasma actuator acted in a position where the unforced boundary

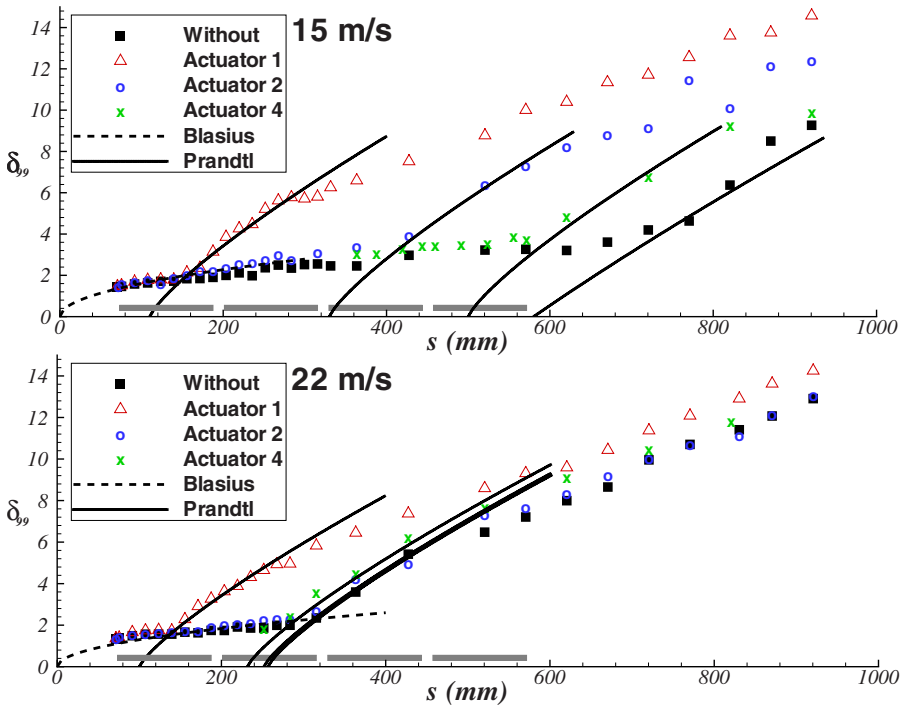

Fig. 12 Boundary layer thickness δ_{99} (mm) along the flat plate for 15 m/s and 22 m/s, for various DBD actuator positions (±8 kV, 1 kHz)

layer was turbulent (s=463 mm), there was no significant effect on the flow for ±8 kV and 1 kHz. For example, boundary layers were not significantly modified above the second plasma actuator when this one was activated. As shown in Fig. 17, nondimensional mean velocity profiles were slightly modified for 22 m/s when the second or the fourth plasma actuator acted on a turbulent flow.

In order to modify a turbulent boundary layer, several high voltages were applied to the actuator, from ±6 kV to ±12 kV and 1 kHz. The boundary layer was mechanically tripped by a turbulator placed in s=100 mm, and the boundary layer for 15

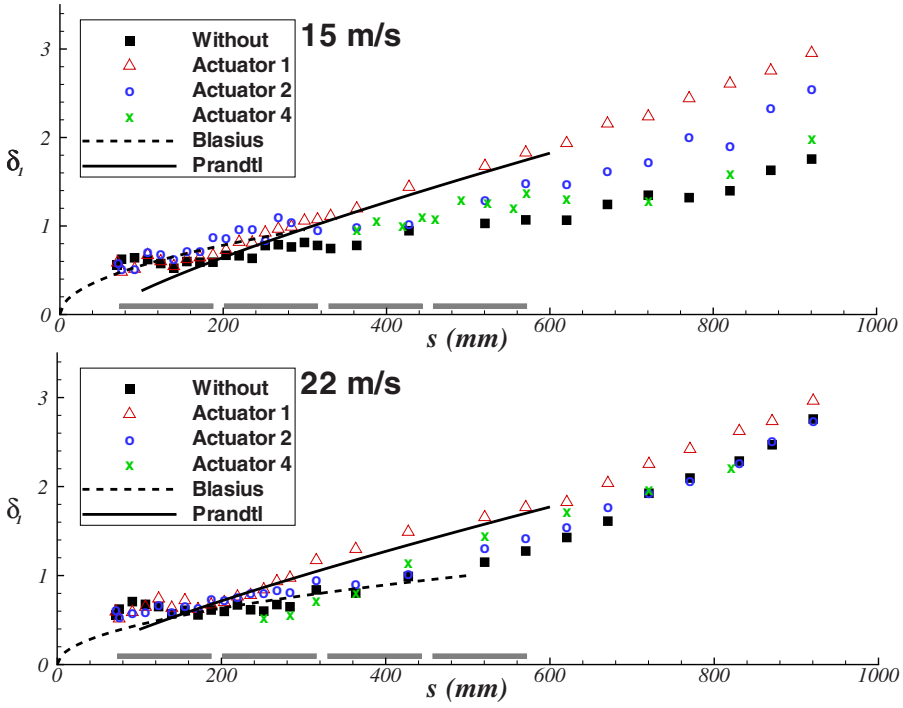

Fig. 13 Displacement thickness δ_1 (mm) along the flat plate for 15 m/s and 22 m/s, for various DBD actuator positions (±8 kV, 1 kHz)

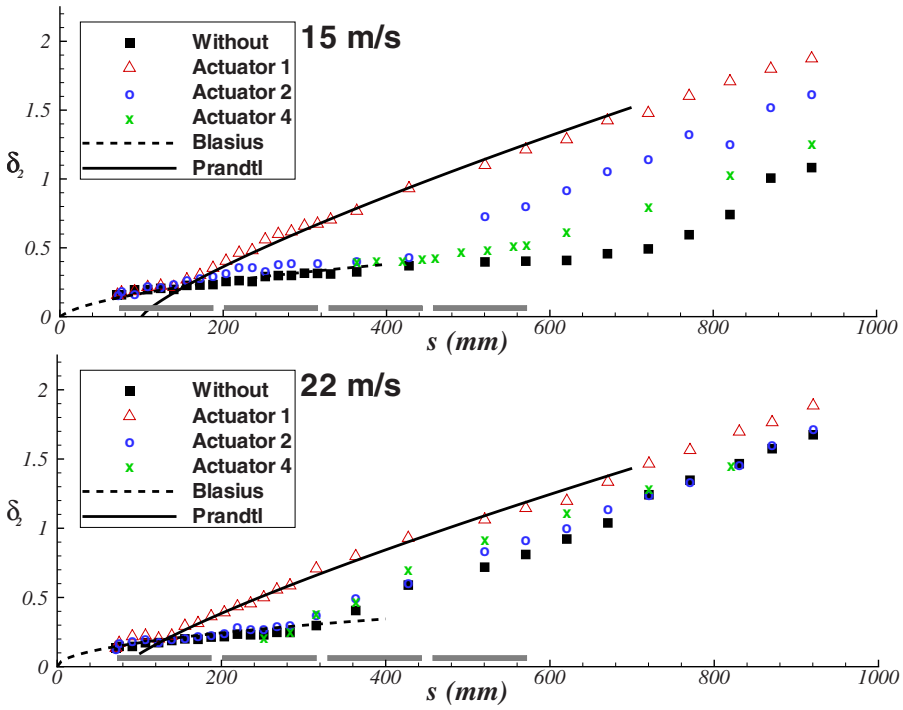

Fig. 14 Momentum thickness δ_2 (mm) along the flat plate for 15 m/s and 22 m/s, for various DBD actuator positions (±8 kV, 1 kHz)

m/s was consequently turbulent above the third actuator. The comparison of velocity profiles measured in $s=446$ mm, 1 mm behind the last pair of electrodes of this actuator (same position as the induced velocity profiles in Sec. 3.1), is shown in Fig. 18. The various boundary layer parameters are reported in Table 3 where the difference in percentage is calculated between the cases without and with a working actuator.

From this experiment, we expected a momentum addition on the velocity profiles related to a decrease in the momentum thickness δ_2, since we increased the actuator active power and then the

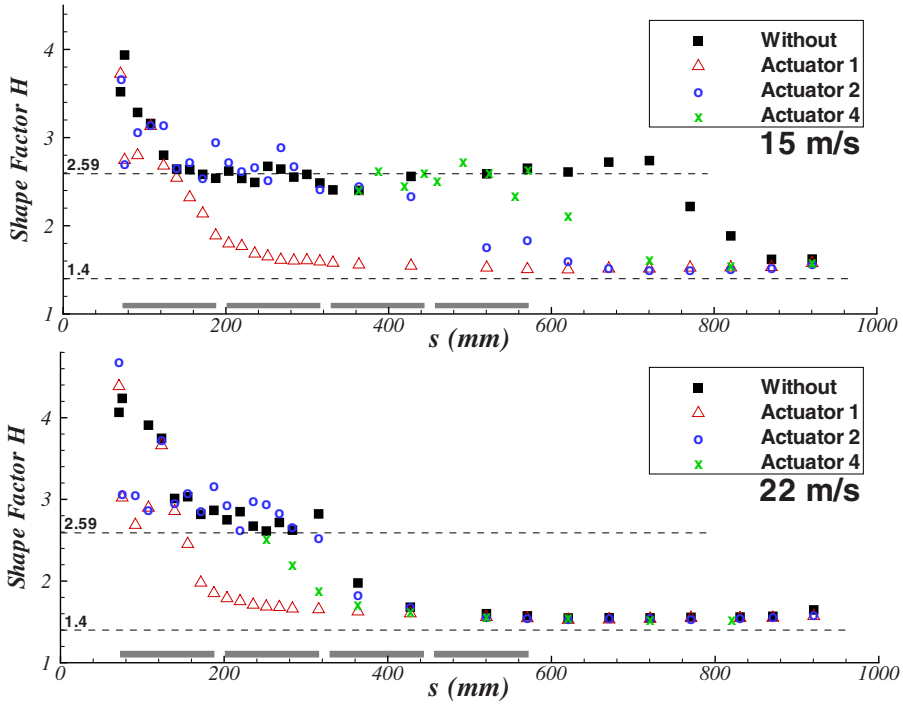

Fig. 15 Shape factor *H* along the flat plate for 15 m/s and 22 m/s, for various DBD actuator positions (±8 kV, 1 kHz)

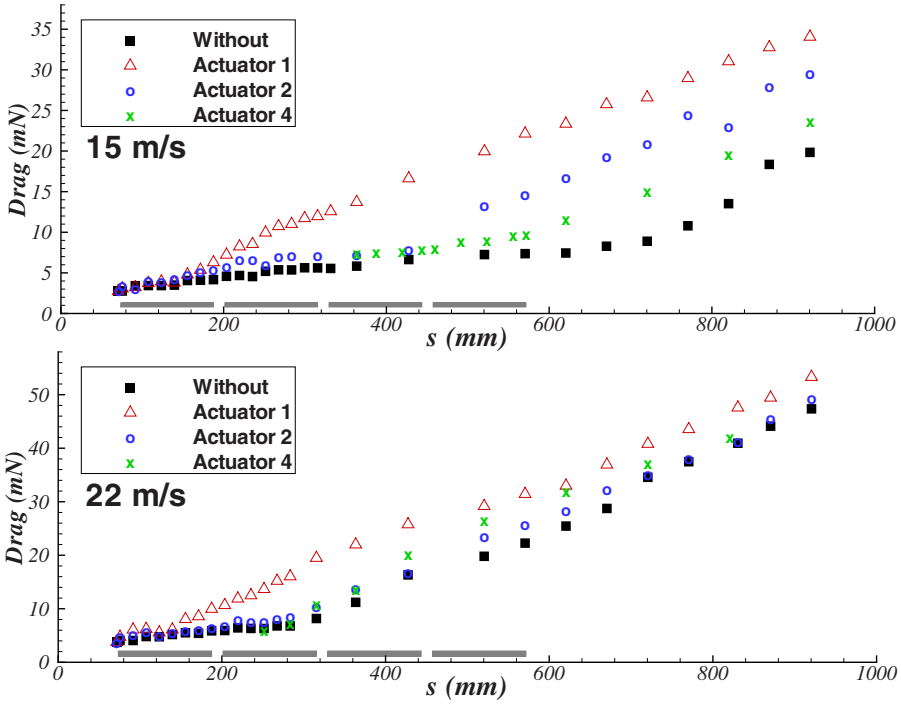

Fig. 16 Drag *D* (mN) along the flat plate for 15 m/s and 22 m/s, for various DBD actuator positions (±8 kV, 1 kHz)

Table 2 Position of the turbulent boundary layer for 15 m/s and 22 m/s, without and with activated actuators 1, 2, or 4 (±8 kV, 1 kHz)

15 m/s	s_t (mm)
Without	580
Actuator 1	110
Actuator 2	330
Actuator 4	500
22 m/s	**s_t (mm)**
Without	255
Actuator 1	100
Actuator 2	250
Actuator 4	240

ionic wind velocity (as shown in Table 1). However we noticed an increase in this parameter, as well as an increase in the boundary layer thickness δ_{99}. The natural turbulent velocity profile was modified in the first millimeter, as shown in Fig. 18, since the plasma induced a momentum addition very close to the wall (Fig. 7). As the values of δ_{99}, δ_1, and δ_2 increased, the effect of plasma actuation was to enhance turbulence in the boundary layer. Moreover, for higher discharge voltages the modified boundary layer was increasingly turbulent. Indeed, as shown in Sec. 3, more ionized plasma induce faster and thicker ionic wind. Therefore the more that the thickness of the plasma influence is large and strong, the more that its action on a velocity profile is important.

Finally, our plasma actuator with a too low momentum addition cannot significantly modify a turbulent boundary layer. A higher voltage of ±12 kV was applied to the actuator but was too important for this actuator configuration. After a few minutes of activation, the powerful plasma generated electric arcs, which damaged the dielectric and occurred a very short actuator lifespan.

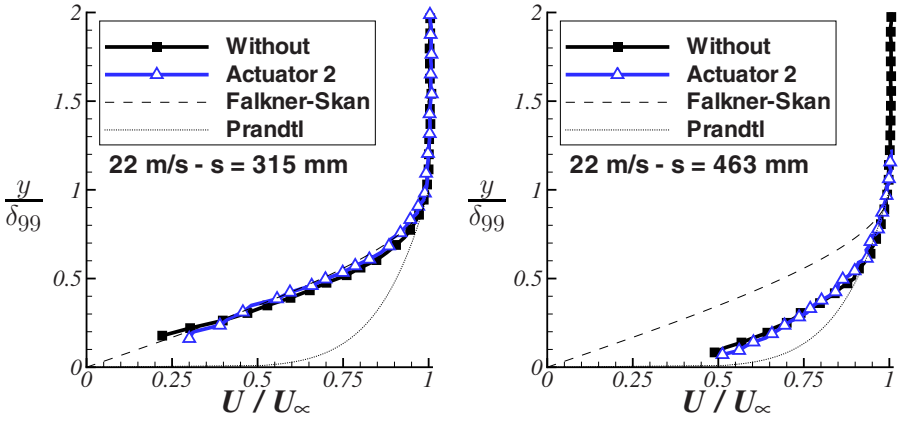

Fig. 17 Velocity profiles for 22 m/s, without and with actuator 2 activated (±8 kV, 1 kHz), in *s*=315 mm and 463 mm

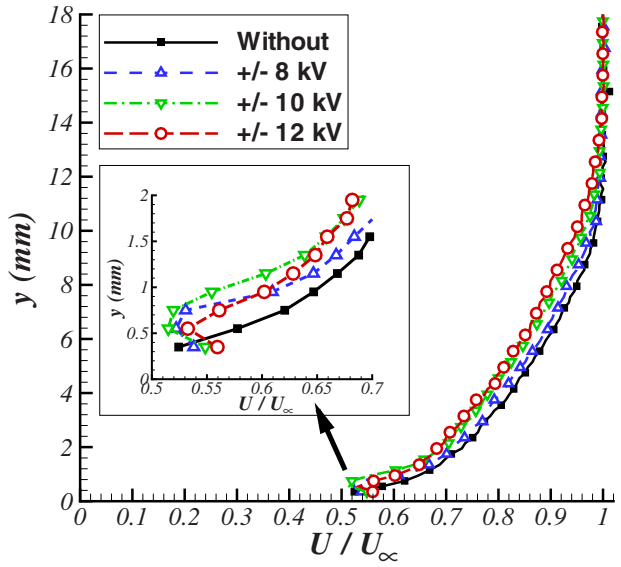

Fig. 18 Velocity profiles in s=446 mm for 15 m/s, with promoted transition, without and with actuator 3 activated (from ±8 kV to ±12 kV, 1 kHz)

5 Conclusion

In the present investigation, a plasma actuator with successive single dielectric barrier discharges was developed. With a pressure sensing probe and PIV visualizations, the ionic wind induced by the actuator was characterized. The higher the frequency and the applied voltage were, the faster was the induced flow downstream of the last pair of electrodes. After each single DBD, the induced velocity increased, and swirls observed between two pairs of electrodes decreased.

Effects of this actuator on a natural evolving boundary layer at zero incidence were studied on a 1-m long flat plate for 15 m/s and 22 m/s. For a moderate applied voltage (±8 kV, 1 kHz), this actuator acted on laminar boundary layers. Flow instabilities were promoted by the ionic wind induced by the DBDs, and the laminar-to-turbulent transition was precociously tripped farther upstream of the unforced case. However, with these applied electric signal conditions, the actuator had no significant effect on turbulent boundary layers.

Higher applied voltages (up to ±12 kV) were applied for modifying turbulent boundary layers. Velocity profiles were modified by the action of the plasma. Thickness and velocity maximum values of the ionic wind are parameters, which are to be considered for an optimization of the actuator effects in the case of turbulent boundary layers.

From these experiments and considering this actuator setup, two kinds of action on wall-bounded subsonic flows can be considered. The first one is to add momentum on the boundary layer. One can thus act everywhere on the surface, whatever the flow regime. However, this type of action requires important applied voltage and power, limiting the lifespan of actuators. The second kind of action is to operate on the laminar-to-transition boundary layer such as in Ref. [15]. In this context, if several actuators are successively mounted along the body surface, boundary layer transition could be tripped everywhere on the surface. Moreover, this last control strategy involves moderate power consumption.

Table 3 Boundary layer parameters in s=446 mm for 15 m/s, with promoted transition, without and with actuator 3 activated (1 kHz and various applied voltages)

	δ_{99}		δ_1		δ_2	
15 m/s	mm	%	mm	%	mm	%
Without	10.45	—	1.52	—	1.17	—
±6 kV	10.73	+2.7	1.54	+1.6	1.18	+1.2
±8 kV	11.59	+10.9	1.71	+12.2	1.28	+9.5
±10 kV	11.89	+13.8	1.94	+27.8	1.43	+22.5
±12 kV	12.92	+23.6	2.05	+35.0	1.54	+31.4

Acknowledgment

This work benefited from the financial support of the research federation EPEE (CNRS/SPI—Orleans University) and the Région Centre in France. Authors would like to thank Stéphane Loyer for his assistance in setting up these experiments.

Nomenclature

A = anode
D = drag
H = shape factor
K = cathode
Re = Reynolds number
s = curvilinear abscissa
s_t = position of the turbulent zone
u = velocity
u^+ = nondimensionalized wall velocity
u_τ = friction velocity
U_p = induced flow maximum velocity
U_∞ = inlet velocity
y = height
y^+ = nondimensionalized wall height
δ_1 = displacement thickness
δ_2 = momentum thickness
δ_{99} = boundary layer thickness
ρ = air density
τ_w = wall shearing-stress
μ = dynamic viscosity
ν = cinematic viscosity

References

[1] Lee, S. J., and Jang, Y. G., 2005, "Control of Flow Around a NACA 0012 Airfoil With a Micro-Ribblet Film," J. Fluids Struct., **20**, pp. 659–672.
[2] Lin, J. C., 2002, "Review of Research on Low-Profile Vortex Generators to Control Boundary-Layer Separation," Prog. Aerosp. Sci., **38**, pp. 389–420.
[3] Modi, V. J., 1997, "Moving Surface Boundary-Layer Control: A Review," J. Fluids Struct., **11**, pp. 627–663.
[4] Greenblatt, D., and Wygnanski, I. J., 2000, "The Control of Separation by Periodic Excitation," Prog. Aerosp. Sci., **36**, pp. 487–545.
[5] Liu C., and Roth, J. R., 1994, "Applications of the One Atmosphere Glow Discharge Plasma to Illumination and Aerodynamic Boundary Layer Control," 36th Annual Meeting APS Division of Plasma Physics, Minneapolis, APS Bulletin, **39**(7), p. 1730.
[6] Robinson, M., 1961, "Movement of Air in the Electric Wind of a Corona Discharge," Trans. Am. Inst. Electr. Eng., **80**, pp. 143–150.
[7] Soetomo, F., 1992, "The Influence of High Voltage Discharge on Flat Plate Drag at Low Reynolds Number Air Flow," M.S. thesis, Iowa State University, Ames.
[8] Artana, G., D'Adamo, J., Desimone, G., and Diprimio, G., 2000, "Air Flow Control With Electrohydrodynamic Actuators," Second International Workshop on Conduction Convection and Breakdown in Fluid, Grenoble, France, pp. 190–194.
[9] Artana, G., Desimone, G., and Touchard, G., 1999, "Study of the Changes in the Flow Around a Cylinder Caused by Electroconvection," *Electrostatics '99*, IOP, Bristol, Philadelphia, pp. 147–152.
[10] Sosa, R., and Artana, G., 2006, "Steady Control of Laminar Separation Over Airfoils With Plasma Sheet Actuators," J. Electrost., **64**, pp. 604–610.
[11] Leger, L., Moreau, E., Artana, G., and Touchard, G., 2001, "Influence of a DC Corona Discharge on the Airflow Along an Inclined Flat Plate," J. Electrost., **51–52**, pp. 300–306.
[12] Leger, L., Moreau, E., and Touchard, G., 2002, "Effect of a DC Corona Electrical Discharge on the Airflow Along a Flat Plate," IEEE Trans. Ind. Appl., **38**(6), pp. 1478–1485.
[13] Leger, L., Moreau, E., and Touchard, G., 2002, "Electrohydrodynamic Airflow Control Along a Flat Plate by a DC Surface Corona Discharge—Velocity Profile and Wall Pressure Measurements," AIAA Paper No. 2002-2833.
[14] Magnier, P., Hong, D., Leroy-Chesneau, A., Pouvesle, J. M., and Hureau, J., 2007, "A DC Corona Discharge on a Flat Plate to Induce Air Movement," J.

Electrost., **65**(10–11), pp. 655–659.
[15] Magnier, P., Hong, D., Leroy-Chesneau, A., Bauchire, J. M., and Hureau, J., 2007, "Control of Separated Flows With the Ionic Wind Generated by a DC Corona Discharge," Exp. Fluids, **42**(5), pp. 815–825.
[16] Roth, J. R., Sherman, D. M., and Wilkinson, S. P., 1998, "Boundary Layer Flow Control With a One Atmosphere Uniform Glow Discharge Surface Plasma," AIAA Paper No. 98-0328.
[17] Roth, J. R., Sin, H., Madhan, R. C. M., and Wilkinson, S. P., 2003, "Flow Re-Attachment and Acceleration by Paraelectric and Peristaltic Electrohydrodynamic (EHD) Effects," AIAA Paper No. 2003-0351.
[18] Roth, J. R., and Dai, X., 2006, "Optimization of the Aerodynamic Plasma Actuator as an Electrohydrodynamic (EHD) Electrical Device," AIAA Paper No. 2006-1203.
[19] Enloe, C. L., McLaughlin, T. E., Van Dyken, R. V., Kachner, K. D., Jumper, E. J., and Corke, T. C., 2003, "Mechanisms and Responses of a Single Dielectric Barrier Plasma," AIAA Paper No. 2003-1021.
[20] Enloe, C. L., McLaughlin, T. E., Van Dyken, R. V., Kachner, K. D., Jumper, E. J., and Corke, T. C., 2004, "Mechanisms and Responses of a Single Dielectric Barrier Plasma Actuator: Geometric Effects," AIAA J., **42**(3), pp. 595–604.
[21] Enloe, C. L., McLaughlin, T. E., Van Dyken, R. V., Kachner, K. D., Jumper, E. J., and Corke, T. C., 2004, "Mechanisms and Responses of a Single Dielectric Barrier Plasma Actuator: Plasma Morphology," AIAA J., **42**(3), pp. 589–594.
[22] Pons, J., Moreau, E., and Touchard, G., 2005, "Asymmetric Surface Dielectric Barrier Discharge in Air at Atmospheric Pressure: Electrical Properties and Induced Airflow Characteristics," J. Phys. D, **38**, pp. 3635–3642.
[23] Sosa, R., Moreau, E., Touchard, G., and Artana, G., 2004, "Stall Control at High Angle of Attack With Periodically Excited EHD Actuators," AIAA Paper No. 2004-2738.
[24] Corke, T. C., and Post, M. L., 2005, "Overview of Plasma Flow Control: Concepts, Optimization and Applications," AIAA Paper No. 2005-0563.
[25] Corke, T. C., Merts, B., and Patel, M. P., 2006, "Plasma Flow Control Optimized Airfoil," AIAA Paper No. 2006-1208.
[26] Post, M. L., Greenwade, S. L., Yan, M. H., Corke, T. C., and Patel, M. P., 2007, "Effects of an Aerodynamic Plasma Actuator on an HSNLF Airfoil," AIAA Paper No. 2007-638.
[27] Opaits, D. F., Roupasov, D. V., Starikovskaia, A. Y., Zavialov, I. N., and Saddoughi, S. G., 2005, "Plasma Control of Boundary Layer Using Low-Temperature Non Equilibrium Plasma of Gas Discharge," AIAA Paper No. 2005-1180.
[28] Moreau, E., 2007, "Airflow Control by Non Thermal Plasma Actuators," J. Phys. D, **40**, pp. 605–636.
[29] Sosa, R., 2007, "Mecanismos de Acople en Actuadores EHD," Ph.D. thesis, University of Buenos Aires, Buenos Aires, Argentina.
[30] Velkoff, H., and Ketcham, J., 1968, "Effect of an Electrostatic Field on Boundary Layer Transition," AIAA J., **16**(7), pp. 1381–1383.
[31] Grundmann, S., and Tropea, C., 2007, "Experimental Transition Delay by Using Glow-Discharge Plasma Actuators," Exp. Fluids, **42**(4), pp. 653–657.
[32] Moreau, E., Léger, L., and Touchard, G., 2006, "Effect of a DC Surface-Corona Discharge on a Flat Plate Boundary Layer for Air Flow Velocity Up to 25 m/s," J. Electrost., **64**(3–4), pp. 215–225.
[33] Porter, C. O., McLaughlin, T. E., Enloe, C. L., Font, G. I., Roney, J., and Baughn, J. W., 2007, "Boundary Layer Control Using a DBD Plasma Actuator," AIAA Paper No. 2007-786.
[34] Vilela Mendes, R., and Dente, J. A., 1998, "Boundary-Layer Control by Electric Fields," ASME J. Fluids Eng., **120**, pp. 626–629.
[35] Visbal, M. R., Gaitonde, D. V., and Roy, S., 2006, "Control of Transitional and Turbulent Flows Using Plasma-Based Actuators," AIAA Paper No. 2006-3230.
[36] Van Dyken, R. V., Enloe, C. L., and McLaughlin, T. E., 2004, "Parametric Investigations of a Single Dielectric Barrier Plasma Actuator," AIAA Paper No. 2004-0846.
[37] Likhanskii, A. V., Schneider, M. N., Macheret, S. O., and Miles, R. B., 2006, "Modeling of Interaction Between Weakly Ionized Near-Surface Plasmas and Gas Flow," AIAA Paper No. 2006-1204.
[38] Borghi, C. A., Carraro, M. R., and Cristofolini, A., 2005, "Plasma and Flow Characterization in a Flat Panel One Atmosphere Uniform Barrier Discharge," AIAA Paper No. 2005-5307.
[39] Forte, M., Jolibois, J., Moreau, E., Touchard, G., and Cazalens, M., 2006, "Optimization of a Dielectric Barrier Discharge Actuator by Stationary and Non-Stationary Measurements of the Induced Flow Velocity—Application to Airflow Control," AIAA Paper No. 2006-2863.
[40] Magnier, P., Dong, B., Hong, D., Bauchire, J. M., Hureau, J., and Pouvesle, J. M., 2006, "Dielectric Barrier Discharge for Airflow Control," Proceedings of the International Symposium on Electrohydrodynamics, Buenos Aires, Argentina, pp. 63–66.
[41] Schlichting, H., 1968, *Boundary-Layer Theory*, 6th ed., McGraw-Hill, New York.
[42] Boeuf, J. P., Lagmich, Y., Unfer, T., Callegari, T., and Pitchford, L. C., 2007, "Electrohydrodynamic Force in Dielectric Barrier Discharge Plasma Actuators," J. Phys. D, **40**, pp. 652–662.